JOURNAL OF GUIDANCE, CONTROL, AND DYNAMICS
Vol. 19, No. 1, January–February 1996

Robust Control Design Framework for Substructure Models

Kyong B. Lim*
NASA Langley Research Center, Hampton, Virginia 23665

A framework for designing control systems directly from substructure models and uncertainties is proposed. The technique is based on combining a set of substructure robust control problems by an interface stiffness matrix that appears as a constant gain feedback. Variations of uncertainties in the interface stiffness are treated as a parametric uncertainty. It is shown that multivariable robust control can be applied to generate centralized or decentralized controllers that guarantee performance with respect to uncertainties in the interface stiffness, reduced component modes, and external disturbances. The technique is particularly suited for large, complex, and weakly coupled flexible structures.

I. Introduction

A. Problem Motivation

THE motivation for studying this problem can be explained by considering the docking of the Shuttle with a space station as shown in Fig. 1. For the purpose of this study, we define the process of stiffness coupling between the Space Shuttle and station as docking. It should be noted that the coupling process is much more complicated than is assumed in this study; for example, see Refs. 1–3. During docking or joining of structures in space, a significant problem to be considered is the stabilization of the coupled system before, during, and after the docking of the two systems. An additional complication faced by the engineer is the difficulty in accurately predicting the dynamics of the coupled system because of the complexity in the physics of the interface or docking mechanism.

A further motivation for this work arises from the peculiar problem faced by the engineer in the development and validation of design models for a large flexible structure, such as the space station. Because of the 1-g testing environment, it may not be possible to test the assembled structure on the ground and so only components can be tested. This means that only models of substructures can be refined directly using experimental data. Component testing, however, can be used to develop substructure uncertainty models arising from inadequate or incomplete component modes and inconsistencies in the substructure boundary conditions.

B. Relation to Previous Work

From the viewpoint of large-scale systems theory, many relevant results exist. Early results in Ref. 4 derive conditions for the existence of robust decentralized controllers for general linear, time-invariant, interconnected subsystems. The controllers are assumed decentralized in the sense of local output feedback structure. Stability robustness is considered, but a quantitative treatment of robustness is not given. The extension in Ref. 5 of the existence conditions to large flexible space structures are for collocated sensors and actuators. The results are further relaxed in Ref. 6 so that collocated sensors and actuators are not necessary. The existence conditions are used to guide the choice of actuators and sensors needed, which is then followed by parameter optimization to obtain controller gains. Another decentralized controller configuration that is closely related to the class of dissipative controllers is developed for large flexible space structures in Refs. 7 and 8. The results in Ref. 9 incorporate subsystem disturbance/performance variables and modeling uncertainties for a general interconnected system; controller existence conditions are derived, and a discussion of the effect of structured uncertainty on stability robustness is given. It is, however, not clear how optimal robust controllers can be obtained.

From the viewpoint of structural modeling, several recent methods for decentralized control of large flexible structures that are based on finite-elements and component modes synthesis exist. A technique whereby substructure controllers for each structural component are independently designed and then synthesized is given in Ref. 10. The independent substructure controller designs are dependent on approximating the interface boundary conditions and component modeling of its adjacent components. To improve the approximation, internal boundary motion is minimized by feedback control. This method, in general, does not guarantee nominal stability, and the report cites robustness issues as a current research direction, clearly recognizing inevitable component modeling errors. A substructure controller synthesis technique is proposed in Refs. 11 and 12 whereby the controller is an assembly of subcontroller designs based on individual uncoupled substructures. As in Ref. 10, however, closed-loop stability is not guaranteed when the substructures are connected. This is not unexpected because the interface stiffness coupling is not taken into account in the synthesis. More recently, a substructure-based controller design approach has been proposed.[13] The basic idea is to combine a set of optimal component controllers that are designed independently. Recognizing the influence of neighboring substructures, the substructure plant used in the control design is appended by a simplified model of neighboring substructure dynamics. Although this approach is computationally efficient, in general, closed-loop stability is not guaranteed. In summary, note that since all structural models or, for that matter, all mathematical models are approximations of physical systems, controllers that guarantee robust stability have a clear advantage over controllers that do not.

Although the previous work just described by no means represents all pertinent past results in the open literature, several issues appear to remain unresolved. Among these that are addressed in this paper are accounting for component modeling errors, variations, and/or undermodeling or modeling errors in the substructure interface, and performance robustness. As will be evident, the proposed framework

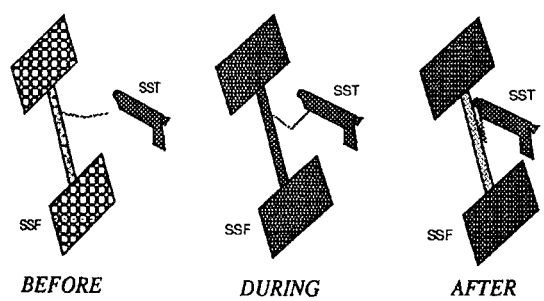

Fig. 1 Docking/berthing of shuttle and station.

Received April 12, 1994; revision received June 2, 1995; accepted for publication June 19, 1995. Copyright © 1995 by the American Institute of Aeronautics and Astronautics, Inc. No copyright is asserted in the United States under Title 17, U.S. Code. The U.S. Government has a royalty-free license to exercise all rights under the copyright claimed herein for Governmental purposes. All other rights are reserved by the copyright owner.

*Research Engineer, Guidance and Control Branch, Flight Dynamics and Control Division. Member AIAA.

amounts to an integration of well-established results in substructure modeling and recent advances in multivariable robust control. The advantages in this synergism include 1) nominal model and uncertainties at the substructure level can be incorporated directly for control analysis and design and 2) a class of problems involving variable stiffness coupling between various structural systems can be treated conveniently. This approach allows substructure or component mode synthesis dynamic models (for example, see Refs. 14–17) to be used directly in the analysis and design of control systems. Perhaps the major advantage in this approach is the reduction in dependence on on-orbit system identification testing of the assembled structure by using easier and less costly testing of substructures on the ground.

C. Organization of Paper

Section II outlines briefly the dynamic model of substructures that is then used in Sec. III to define the uncoupled substructure robust control problem (SRCP) in the framework of modern multivariable robust control. A novel element in Secs. II and III is the inclusion of substructure boundary forces/moments as external disturbances on the substructure and the usage of the displacement and rotations at the substructure boundaries as substructure output variables. The nominal substructure model and the associated uncertainties are defined along with the input and output control variables for the substructure. In Sec. IV, a model for stiffness coupling is introduced and the substructure interface stiffness matrix is defined. This interface stiffness matrix can be viewed as a transfer function matrix that maps the displacements and rotations at the interface to the corresponding interface forces and moments. Section IV shows how displacements and rotations at the interface can be realized into a block diagram form suitable for connecting subsystems. For the case where the substructure interface involves a variable and/or unknown stiffness coupling, the interface conditions can be treated as a parametric uncertainty in a multivariable robust control framework. In principle, this interface block could be extended to include certain or uncertain dynamic models. In Sec. V, the control problem for the connected system is defined by connecting the SRCP using the substructure interface block. To demonstrate the utility of the ideas introduced in this paper, a sequence of control design examples involving controller designs for two connected flexible beams are outlined in Sec. VI; Sec. VII contains a few concluding remarks.

II. Substructure Model

The following formulation is discussed in more detail in Refs. 15 and 16. Let $M^{(i)}$ and $K^{(i)}$ denote the mass and stiffness matrices corresponding to the ith substructure so that the finite element model is given by

$$M^{(i)}\ddot{\xi}^{(i)} + K^{(i)}\xi^{(i)} = D_u^{(i)}u^{(i)} + D_I^{(i)}g^{(i)} + D_r^{(i)}r^{(i)} \tag{1}$$

where $\xi^{(i)}$ is the physical nodal displacement vector. For substructure i, the matrices $D_u^{(i)}$, $D_I^{(i)}$, and $D_r^{(i)}$ are the force/moment distribution matrix for control input $u^{(i)}$, the substructure interface input distribution matrix for interface forces/moments $g^{(i)}$, and the force/moment distribution matrix for external command and/or disturbances $r^{(i)}$, respectively. It is important to note that in component mode synthesis, the interface forces and moments are not included or carried through in the substructure equations because they are absorbed in the synthesis process as internal forces and moments. The explicit consideration of these internal variables at the substructure interfaces, however, is a key ingredient in the SRCP formulation.

The substructure eigenvalue problem for substructure i, for an assumed set of boundary conditions, is given by

$$K^{(i)}\psi_j^{(i)} = \lambda_j M^{(i)}\psi_j^{(i)} \tag{2}$$

where j is the structural mode number. Using only a subset of substructure or component modes $\Psi^{(i)}$ where

$$\xi^{(i)} = \Psi^{(i)}\eta^{(i)} + \Psi_{\text{tr}}^{(i)}\eta^{(i)} \tag{3}$$

the Ritz approximation leads to the substructure reduced modal model,

$$\ddot{\eta}^{(i)} + \Omega^{(i)^2}\eta^{(i)} = \Psi^{(i)T}D_u^{(i)}u^{(i)} + \Psi^{(i)T}D_I^{(i)}g^{(i)} + \Psi^{(i)T}D_r^{(i)}r^{(i)} \tag{4}$$

where $\eta^{(i)}$ is the modal amplitude vector and $\Omega^{(i)^2} = \text{diag}\,(\omega_1^{(i)^2}, \ldots, \omega_n^{(i)^2})$. The columns of $\Psi_{\text{tr}}^{(i)}$ denote truncated modeshapes for substructure i.

In general, the synthesized component modes model do not lead to a model with sufficient fidelity when only the truncated sets of normal component modes [represented by $\Psi^{(i)}$ in Eq. (3)] are used in the synthesis. Therefore, the reduced set of normal component modes are typically augmented with constraint modes. For a more comprehensive treatment on adding constraint modes to normal modes, Ref. 15 is recommended. Indeed, the selection of a subset of component modes or assumed shape functions is an important element in substructure synthesis and the work in Refs. 13 and 17 is recommended for a more detail discussion.

In the sections to follow, the effect of the truncated substructure modes $\Psi_{\text{tr}}^{(i)}\eta^{(i)}$ in Eq. (3) (i.e., the Ritz approximation error) are included as additive uncertainties about the nominal model. The closed-loop robustness is partly with respect to this model error. It is significant to note that if the entire set of component modes span the entire substructure configuration vector space, a Ritz approximation plus the additive uncertainty will be sufficient to span this vector space. An implication of this truth is that potential spillover into the truncated modes can be properly accounted for in the control design, although closed-loop performance is limited by the inaccurate set of reduced normal modes.

The displacement and velocity outputs for substructure i are given by

$$y^{(i)} = \begin{Bmatrix} y_d^{(i)} \\ y_v^{(i)} \end{Bmatrix} = \begin{bmatrix} D_d^{(i)T}\xi^{(i)} \\ D_v^{(i)T}\dot{\xi}^{(i)} \end{bmatrix} \tag{5}$$

$$\approx \begin{bmatrix} D_d^{(i)T}\Psi^{(i)} & \\ & D_v^{(i)T}\Psi^{(i)} \end{bmatrix} \begin{Bmatrix} \eta^{(i)} \\ \dot{\eta}^{(i)} \end{Bmatrix} \tag{6}$$

The displacement and rotation at the interface for substructure i are

$$\xi_b^{(i)} = D_b^{(i)}\xi^{(i)} \tag{7}$$

$$\approx D_b^{(i)T}\Psi^{(i)}\eta^{(i)} \tag{8}$$

Each column of $D_b^{(i)}$ corresponds to the individual interface degree-of-freedom (DOF) location for substructure i. The outputs of interest are written as

$$e^{(i)} = \begin{bmatrix} D_{e_d}^{(i)T} & D_{e_v}^{(i)T} \end{bmatrix} \begin{Bmatrix} \xi^{(i)} \\ \dot{\xi}^{(i)} \end{Bmatrix} \tag{9}$$

$$\approx \begin{bmatrix} D_{e_d}^{(i)T}\Psi^{(i)} & D_{e_v}^{(i)T}\Psi^{(i)} \end{bmatrix} \begin{Bmatrix} \eta^{(i)} \\ \dot{\eta}^{(i)} \end{Bmatrix} \tag{10}$$

In the field of structural dynamics, the main purpose of substructure modeling via component mode synthesis appears to be the prediction of frequencies, mode shapes and, possibly, damping for the assembled structure. The modular nature of this approach also allows independent structural analysis and refinement and component testing even by separate organizations. Although much attention has been given to the basic problem of component mode selection, issues pertaining to the use of substructure models for controller design has not been fully addressed. As a result, two problems that are addressed in this study are substructure model reduction errors and the modeling of variable or uncertain substructure interface, both in the context of performance robustness of closed-loop coupled substructures.

III. Uncoupled Substructure Robust Control Problem

Define the states for substructure i as

$$x^{(i)} = \begin{pmatrix} \eta_1^{(i)} & \dot{\eta}_1^{(i)} & \ldots & \eta_n^{(i)} & \dot{\eta}_n^{(i)} \end{pmatrix}^T \tag{11}$$

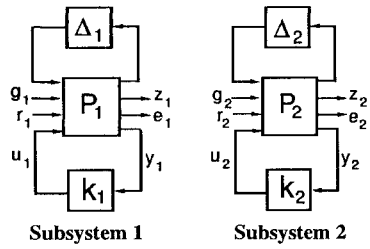

Fig. 2 Uncoupled SRCP for two substructures.

The substructure state equations can be written as

$$\dot{x}^{(i)} = A^{(i)}x^{(i)} + B_1^{(i)}g^{(i)} + B_2^{(i)}r^{(i)} + B_3^{(i)}u^{(i)} \tag{12}$$

The coefficient matrices, $B_1^{(i)}$, $B_2^{(i)}$, and $B_3^{(i)}$, are state space forms of $D_u^{(i)}$, $D_I^{(i)}$, and $D_r^{(i)}$ in Eq. (1). The displacement measurement, pointing error, and interface boundary DOF can be written in terms of substructure state vector

$$\mathbf{y}^{(i)} = C_3^{(i)}x^{(i)} \tag{13}$$

$$\mathbf{e}^{(i)} = C_2^{(i)}x^{(i)} \tag{14}$$

$$\xi_b^{(i)} = C_1^{(i)}x^{(i)} \equiv z_i \tag{15}$$

Similarly, the coefficient matrices, $C_3^{(i)}$, $C_2^{(i)}$, and $C_1^{(i)}$, are the corresponding state space forms of the relevant outputs in Eqs. (5–10). Denote the transfer function matrix of substructure i as

$$G^{(i)} = \begin{bmatrix} A^{(i)} & B^{(i)} \\ C^{(i)} & 0 \end{bmatrix} \tag{16}$$

where

$$B^{(i)} = \begin{bmatrix} B_1^{(i)} & B_2^{(i)} & B_3^{(i)} \end{bmatrix}; \qquad C^{(i)} = \begin{bmatrix} C_1^{(i)} \\ C_2^{(i)} \\ C_3^{(i)} \end{bmatrix} \tag{17}$$

The transfer function matrix of the substructure, $G^{(i)}$, is then appended with weighting matrices that define substructure closed-loop performance and uncertainties peculiar to that substructure to form augmented substructure plant $P_{(i)}$.

For the special case where the substructures are uncoupled (for example, at the onset of docking), Fig. 2 shows the subsystem plants P_1 and P_2, substructure controllers k_1 and k_2, and uncertainties associated with each substructure Δ_1 and Δ_2. Although the following development is based on a system with only two substructures, it should be clear that the methodology presented also applies to a system with an arbitrary number of substructures. The subsystem plants consist of substructure models that are augmented with performance, disturbance, and uncertainty weighting matrices that are used to define the substructure control problem. The uncertainty blocks are assumed to be normalized to unity in terms of their maximum singular values (e.g., see Ref. 18). The structure in the uncertainty block is problem dependent and is selected by the engineer.

The uncoupled SRCP can be described as seeking a controller $k_{(i)}$ that maintains stability and performance for the set of all closed-loop systems defined by the given uncertainty set Δ_i. The performance considered is defined in terms of a suitable frequency-weighted norm of the transfer function matrix, from the disturbances r_1 and r_2 to outputs of interest e_1 and e_2. This form of the performance can physically represent regulation, tracking, and/or disturbance rejection problems.

In general, any suitable multivariable design approach can be used to generate a substructure robust controller. References 7 and 19 describe several control design approaches, including parameter optimization via nonlinear programming. In this paper, we consider the robust performance measure in terms of the structured singular value. The problem then reduces to minimizing μ (e.g., see Refs. 21–23).

IV. Substructure Interface

In this section, a model of a substructure interface is developed for the purpose of formulating the coupled SRCP.

A. Static Interface

Consider the structural interconnection between two substructures. Denote those DOF at the interface boundaries for the two substructures by superscripts (1) and (2) and the stiffness interfaces by superscript (I). The variables $\xi_{b1}^{(1)}, \ldots, \xi_{bm}^{(1)}$ denote the DOF at the interface for substructure 1, whereas $\xi_{b1}^{I/(1)}, \ldots, \xi_{bm}^{I/(1)}$ denote the structural interface DOF adjoining substructure 1. Similarly, the variables $\xi_{b1}^{(2)}, \ldots, \xi_{bm}^{(2)}$ correspond to the DOF at the interface for substructure 2, whereas $\xi_{b1}^{I/(2)}, \ldots, \xi_{bm}^{I/(2)}$ denote the DOF at the adjoining interface structure. The interface stiffness matrix S^I is defined as follows:

$$S^I \begin{Bmatrix} \xi^{I/(1)} \\ \xi^{I/(2)} \end{Bmatrix} = \begin{Bmatrix} f^{I/(1)} \\ f^{I/(2)} \end{Bmatrix} \tag{18}$$

where all of the variables without subscripts denote vector representation of corresponding DOF. As in any stiffness matrix, the (i, j)th element of S^I physically represents the force (or moment) at DOF i due to a unit displacement (or rotation) at DOF j. In the general case where there are DOF internal to the interface substructure itself, the interface stiffness matrix in the boundary input/output form, as in Eq. (18), can be obtained by a static condensation procedure.[24]

As an example of a static substructure interface, consider the attachment of a flexible aircraft wing to its fuselage as shown in Fig. 3. A narrow strip of structure located between the wing and the fuselage can be separately modeled by finite elements just as is done for the main substructures. The symbol $\xi_m^{I/(k)}$ denotes the mth finite element DOF at the physical node shared by the substructure interface and kth substructure. The interface stiffness for this example relates the interface displacements, forces, and rotations, moments, in the same way as Eq. (18) if we let the superscripts (1) and (2) denote the fuselage and wing, respectively.

From a controls perspective, the interface stiffness can be viewed as a collocated, constant gain output feedback of the displacements and rotations at the substructure interface to the forces and moments on the same substructure interface. Figure 4 shows this constant gain feedback block given in terms of forces and moments on the substructures. Note that since the forces (and moments) in the right-hand side of Eq. (18) are the forces (and moments) acting on the stiffness interface, the reaction forces (and moments) on the substructures will be in opposite directions.

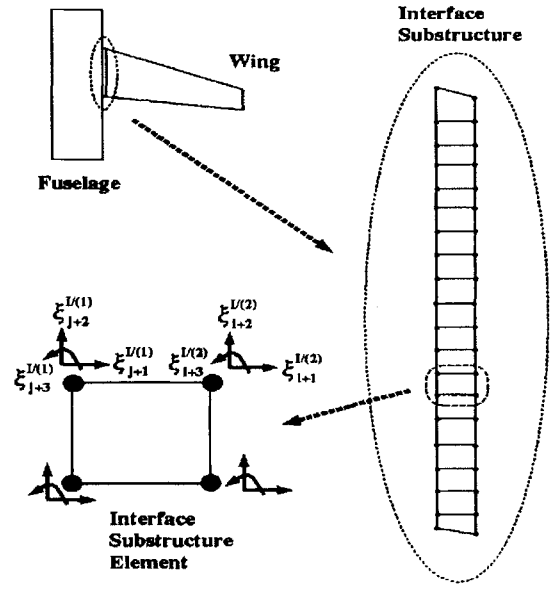

Fig. 3 Structural interface between a wing and its fuselage.

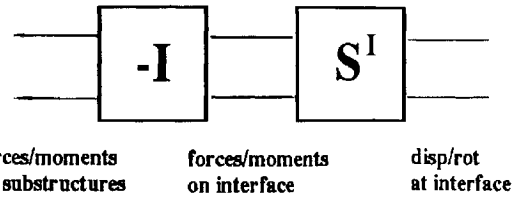

Fig. 4 Substructure interface block diagram.

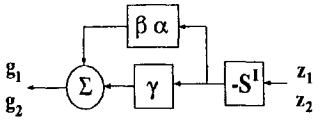

Fig. 5 Interface stiffness uncertainty/variation.

B. Varying/Uncertain Interface

In the event that the substructure interface is uncertain and/or varying, the coupling block can be viewed as a constant linear uncertainty with specified norm bounds. One approach is to model the uncertainty as an independent variation in the interface forces about a nominal stiffness s_0.

For the stiffness interface, let the variation in the interface stiffness be modeled by the following equation between the substructure boundary displacements (and rotations) $(\xi_b^{(1)}, \xi_b^{(2)})$ and the corresponding forces (and moments) (g_1, g_2) on the substructures at the boundaries

$$\begin{Bmatrix} g_1 \\ g_2 \end{Bmatrix} = s \begin{Bmatrix} \xi_b^{(1)} \\ \xi_b^{(2)} \end{Bmatrix} \tag{19}$$

where

$$s = -(\gamma + \beta\alpha)S^I \tag{20}$$

is the effective interface stiffness whereas α, β, and γ are parameters that are defined as follows:

$$|\alpha_i| \leq 1; \qquad i = 1, \ldots, \text{number of boundary DOF} \tag{21}$$

$$\beta_i = \alpha_i^u \tag{22}$$

The parameter γ is a factor appearing in the nominal interface stiffness

$$s_0 = -\gamma S^I \tag{23}$$

Note that when $\gamma = 0$ is selected, it means that the nominal interface stiffness is zero. This, however, does not necessarily imply that the substructures are uncoupled. The combined term $\beta\alpha$ denotes the factor of interface stiffness variation about the nominal. The term α_i^u is the upper limit of change in the ith channel. Note that the ith channel physically corresponds to the ith interface DOF. Figure 5 shows in block diagram form the effective interface stiffness parameterized as a structured uncertainty.

C. Dynamic Interface

So far we have assumed a static model in the form of a stiffness coupling and have formally defined a substructure interface stiffness matrix. In principal, the interface stiffness matrix can be extended to a transfer function matrix that maps the dynamic displacements and rotations at the interface to the corresponding interface forces and moments. In other words, an inverse kinematics model can be developed whereby the kinematic variables (displacements, velocities, and accelerations) at the DOFs adjacent to the substructures are mapped into the corresponding forces and moments.

Similar to the static stiffness interface case, the dynamic interface block could be extended to include certain or uncertain dynamic models. As an example, the interface dynamics associated with a remote manipulator arm between the orbiter and the space station (Fig. 1) could be modeled as a flexible substructure with its own nominal model and uncertainty. More interestingly, it may be sufficient to treat the complex variations due to a slow configuration change in the manipulator arm during docking or when grabbing a payload as a set of plants not different from uncertainty descriptions.

V. Coupled SRCP

In this section, the substructure interface model is combined with the uncoupled SRCP to form a coupled SRCP. It is important to note that a single synthesized model is not formed by removing the interface DOF to predict system frequencies and mode shapes as is traditionally done in component modes synthesis (e.g., see Refs. 15 and 16).

The two substructures connected by a stiffness interface can be represented graphically in block diagram form as shown in Fig. 6. The control objective remains the same as for the uncoupled SRCP, i.e., to optimize disturbance rejection performance under substructure model uncertainties. The objective for coupled SRCP, however, becomes more complicated due to the substructure coupling that may also be slowly varying and/or even uncertain. The disturbance rejection performance is in the form of a suitable frequency weighted norm of the transfer function matrix from the disturbances r_1 and r_2 to outputs of interest e_1 and e_2. The disturbance rejection performance is to be guaranteed under all modeled uncertainties.

Figure 7 shows a general interconnected substructure. The system plant P consists of nominal substructure models $P_1, P_2, \ldots$, whereas the system uncertainty Δ consists of individual substructure uncertainties $\Delta_1, \Delta_2, \ldots$. The system controller K consists of substructure controllers $k_1, k_2, \ldots$. A block-diagonal substructure interface, however, couples the nominal substructures, component uncertainties, and substructure controllers. The width dimension of the block diagonality of interface coupling is dependent on the degree of physical coupling and topology of the interconnections. Notice that even if each of the substructure and interface uncertainties is unstructured, globally, the uncertainties will be highly structured. This is the basis for applying structured singular value

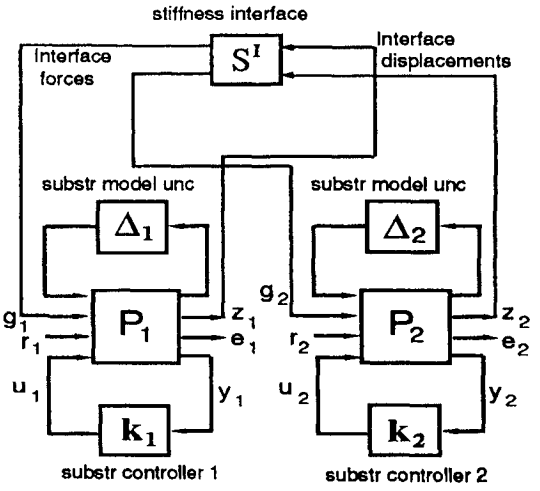

Fig. 6 Stiffness coupled SRCP for two substructures.

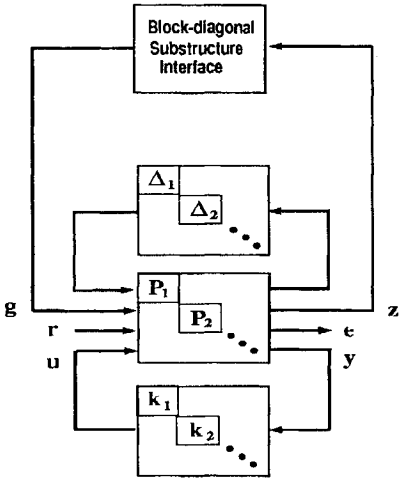

Fig. 7 General coupled SRCP.

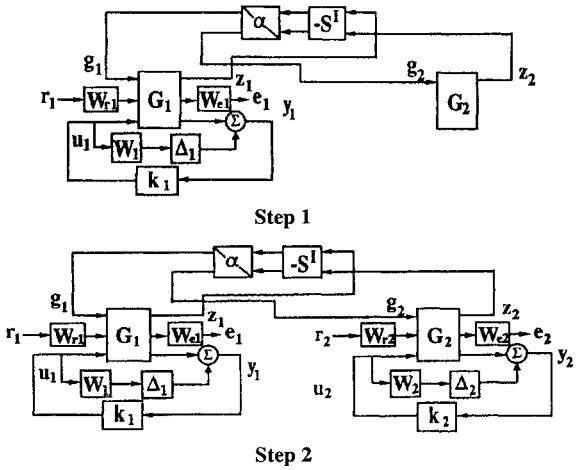

Fig. 8 Design sequence for robust decentralization.

techniques (e.g., see Refs. 20–23) for robust performance controller design in this study.

A. Decentralized Control

Figure 7 shows the decentralized nature of the plant, uncertainty, and controller. The decentralized controller structure (e.g., see Refs. 25–27) is enforced by the classical loop-at-a-time design, namely, design a substructure controller while holding the remaining substructure controllers constant. Figure 8 shows the first two steps of the design sequence to incorporate both robustness and decentralization of the overall system for a system with two substructures.

The first step involves the design of substructure controller k_1, while assuming open loop for substructure 2. At this step, the nominal dynamics of the substructure 2 is included, while the component uncertainty and performance for substructure 2 are ignored. Ignoring the adjacent component's uncertainty and performance is crucial to obtain a reasonable performance controller for substructure 1 because of the localized constraint on substructure controller 1. Accounting for nominal substructure 2 should result in substructure controller 1 that takes into account the primary coupling effects of the neighboring substructure.

In the second step, the controller for substructure 2, k_2, is designed by holding the controller for substructure 1, k_1, constant. The fixed controller k_1 should strongly complement controller k_2 in the control of substructure 2. At this step, all uncertainties and disturbances with the corresponding errors are included. This guarantees performance robustness of the overall system.

Step 3 is similar to step 2 except substructure controller 2 is held constant while substructure controller 1 is refined. Step 4 is the same as step 2 and the sequence follows. For this design example, iterations up to step 3 are carried out for the decentralized control design. In the sequential design process described, the order of the controller will increase with each iteration if the control design technique chosen results in a controller of the same order as the current augmented plant [such as linear quadratic Gaussian (LQG) or central H_∞]. Hence, model order reduction is recommended after each step.

B. Design via μ Synthesis

The disturbance rejection performance from r to e in terms of frequency weighted H_∞ norm is to be guaranteed (or be robust) with respect to a bounded and structured set of component uncertainties Δ_1 and Δ_2 and interface uncertainty Δ_s. The controller can be centralized or decentralized as outlined in the preceding section. The worst-case (over frequency) μ quantifies the degree of robust performance. Designing controllers by μ synthesis involves an iterative minimization of the upper bound using H_∞ methods. The underlying theory that forms the basis of this method is discussed in detail in Refs. 23 and 28–30.

The μ-design problem is summarized as follows:

$$\underset{K,D}{\text{minimize}} \left\| DF_l(P, K)D^{-1} \right\|_\infty \tag{24}$$

where $\{K:F_l(P, K) \in H_\infty\}$, $D \in \underline{D}$. The set of scaling matrices $\underline{D}$ has a similar structure as $\underline{\Delta}$ (the structured uncertainty matrix) with an appended identity matrix. The terms F_l, P, and K are the lower linear fractional transformation, augmented plant, and the controller, respectively. To minimize the weighted H_∞ norm in Eq. (24), the D-K iteration technique is used. In this approach, D or K is optimized independently and sequentially. Optimizing for D while keeping K fixed involves the search for the minimal upper bound on μ, whereas optimizing for K while fixing D involves the minimization of an approximation of μ itself. Although this approach is iterative in nature and convergence to a global minimum is not guaranteed, recent numerical studies show excellent convergence (e.g., see Refs. 21, 31, and 32). The Glover–Doyle algorithm[33,34] is used to solve the H_∞ problem. The MATLAB toolbox, μ-Tools,[22] is used for the analysis and synthesis of the controllers.

VI. Example

A. Description of Structure

Motivated by earlier work on substructure and component mode synthesis, a beam that is cantilevered at both ends is used to illustrate the ideas introduced in this paper. The structure is assumed to consist of two cantilevered Euler–Bernoulli beams joined at the free ends by a short stiffness interface beam element as shown in Fig. 9.

The structural properties and configurations of the beams are given in Table 1. The stiffness and mass density properties are selected such that the resonant frequencies are sufficiently spaced, and the lower frequencies to be controlled are sufficiently small to allow reasonable numerical integration. No deep significance should be attributed to the choice of the numerical values in Table 1 since this is obviously a contrived example to clarify the proposed approach. The beam substructures modeled by 20 and 10 beam elements resulted in 40 and 20 structural modes. The full state space models of the two substructures are then of orders 80 and 40, respectively. The interface stiffness is modeled by a single beam element with four DOF.

The connected structure has 60 structural modes from the total of 31 beam elements. A truncated structural model consisting of the lowest 30 structural modes is used as the evaluation model, and Fig. 10 shows the maximum and minimum singular values of the frequency response matrix from r_1 and r_2 to e_1 and e_2. Note that there is no clear frequency gap where model reduction by modal truncation can be done. It is also clear from the figure that the displacement responses rapidly drop as a function of frequency; this is the basis for modal truncation of higher frequency modes in addition to the well-known inaccuracy of the finite element model in predicting the dynamics at higher frequencies.

B. Control Design

1. Objective

The control objective for this problem is to optimize disturbance rejection performance. In particular, a minimal desired upper bound

Table 1 Structural properties and configuration

Property	Substr. 1	Substr. inter.	Substr. 2
Length	2	0.2	1
Mass density ρ	10	0.1	10
Stiffness EI	10^{-2}	10^{-4}	10^{-2}
No. of elements	20	1	10

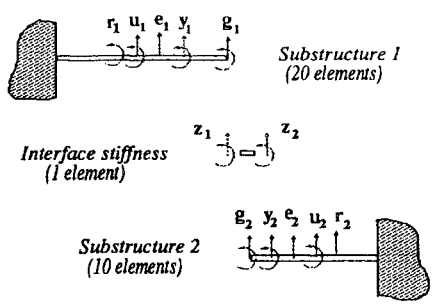

Fig. 9 Joined cantilever beams.

of frequency weighted H_∞ norm of the transfer function matrix from the disturbances r_1 and r_2 to outputs of interest e_1 and e_2 is to be guaranteed under truncated component modes and uncertainties and/or variations in the substructure interface. To optimize the robust performance, μ synthesis is used.

2. Design Configuration

The overall system block diagram is shown in Fig. 11. The model of the two nominal component modes (G_1, G_2), with their corresponding high-frequency truncated modes that are treated as substructure uncertainties ($\Delta_1 W_1$, $\Delta_2 W_2$), is shown. The respective substructure disturbances (r_1 and r_2), and outputs of interests (e_1 and e_2) are also distinguished. The power spectrum of the disturbances are represented by W_{r_1} and W_{r_2}, which frequency weights the all-pass input disturbances. The output error weighting matrices W_{e_1} and W_{e_2} were chosen as unity but, in general, may be chosen to signify their relative importance with respect to other requirements or be frequency weighted. The unstructured uncertainty blocks Δ_1 and Δ_2 and diagonally structured interface stiffness uncertainty block $[\alpha]$ are assumed to be amplitude bounded by unity 2 norm. The interface stiffness block couples the substructures and acts as a constant gain feedback. The controller shown in Fig. 11 is centralized and is used for performance comparisons. Substructure decentralization is defined by $k_{12} = k_{21} = 0$. Figure 12 shows the augmented plant P that includes all performance and uncertainty weights.

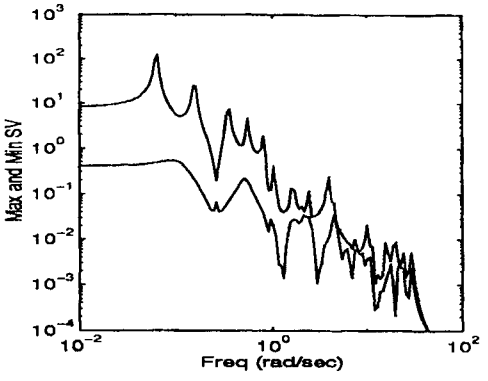

Fig. 10 Frequency response of evaluation model.

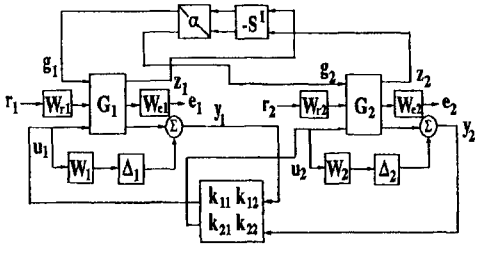

Fig. 11 Block diagram for control design.

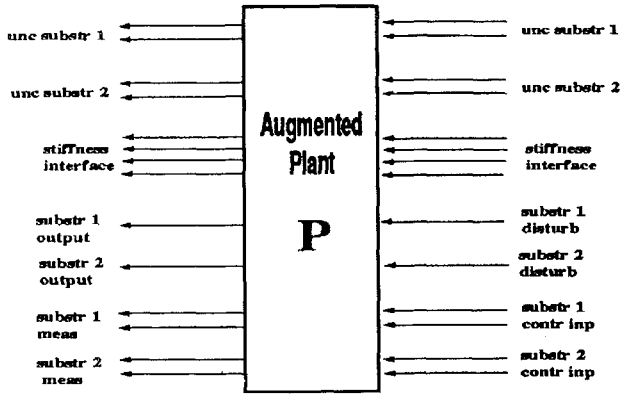

Fig. 12 Augmented plant for μ synthesis.

Table 2 Design configurations, $\beta = 1$

Case no.	Structure interface	Controller
1	$\gamma = 0, \alpha = 0$	$k_{12} = k_{21} = 0$
2	$\gamma = 1, \alpha = 0$	Centralized
3	$\gamma = 1, \alpha = 0$	$k_{12} = k_{21} = 0$
4	$\gamma = 1, \lvert\alpha\rvert \leq 1$	Centralized
5	$\gamma = 1, \lvert\alpha\rvert \leq 1$	$k_{12} = k_{21} = 0$

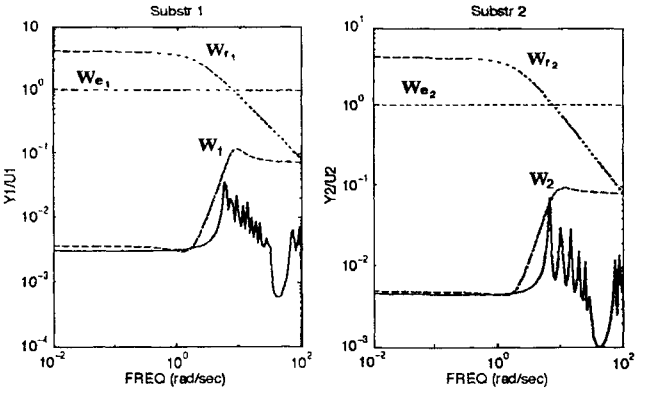

Fig. 13 Substructure uncertainties and weights.

3. Design Weights for SRCP

For all cases, only the lowest eight modes (16 states) for substructure 1 and lowest four modes (8 states) for substructure 2 are targeted for control, whereas the rest of the component modes (32 and 16 modes for substructures 1 and 2) are treated as additive uncertainties. These are normal modes from substructure cantilever boundary conditions. No attempt is made to improve the reduced component modes (nominal) model by adding constraint modes or component shape functions to approximate the residual flexibility. As is typical of flexible structures, most higher frequency component modes are truncated. Figure 13 shows the maximum singular value of the transfer function matrix of the truncated higher frequency component modes (solid line) and a stable, real-rational, second-order weight function used as its upper bound (dotted line) for both substructures. The weights representing upper bounds for substructure uncertainties have the realization

$$W_1 = \left(\begin{array}{cc|c} -2.8622 & -7.5077 & -0.6458 \\ 7.5077 & -2.1794 & 0.4064 \\ \hline 0.6458 & 0.4064 & 0.0735 \end{array}\right) \tag{25}$$

$$W_2 = \left(\begin{array}{cc|c} -5.0127 & -7.1225 & -0.7768 \\ 7.1225 & -2.8930 & 0.3537 \\ \hline 0.7768 & 0.3537 & 0.0819 \end{array}\right) \tag{26}$$

The output weights W_{e_1} and W_{e_2} (dash-dot line) are chosen as unity. The figures also show a first-order frequency weighting function (dashed line), W_{r_1} and W_{r_2}, where

$$W_{r_i} = \frac{s + 1000}{s + 2} * 0.008 \qquad i \in [1, 2] \tag{27}$$

which is representative of the disturbance spectra at r_1 and r_2. They are chosen to reject external disturbances at lower frequencies ($\leq$2 rad/s).

C. Case Studies

Five cases are considered to illustrate the utility of the analysis and design framework based on substructures models as listed in Table 2. The cases are listed in increasing order of design difficulty. In this table, $\gamma = 0$ refers to zero nominal stiffness, whereas α refers to the variation in the interface stiffness. The terms k_{ij}, $i, j \in [1, 2]$ refer to the controller component that maps the measured outputs from substructure j to control inputs of substructure i.

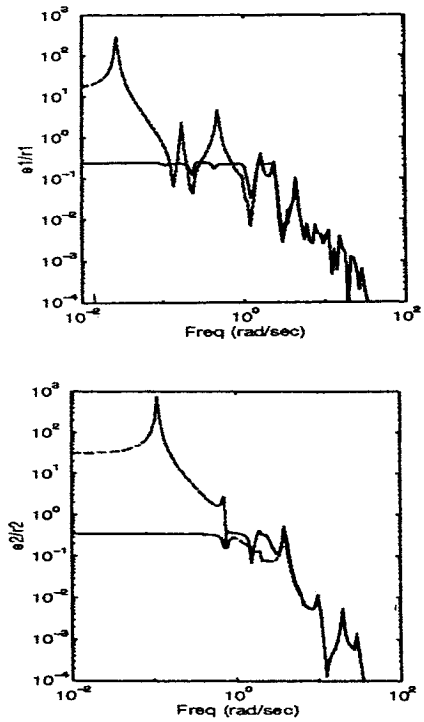

Fig. 14 Frequency response for open loop (dotted line) and closed loop for controller 1 (solid line), $\gamma = \alpha = 0$.

1. Uncoupled SRCP, $\gamma = \alpha = 0$: Case 1

This is the limiting case in performance and simplicity since the subsystems are completely uncoupled. The higher frequency truncated modes of the two substructures are the only model uncertainties assumed in this problem. The weighted frequency response plots in Fig. 14 show that disturbances are rejected very well at the low frequencies by two orders of magnitude over the open-loop response while avoiding spillover. The weighted open- and closed-loop frequency responses were calculated using the full model (80 and 40 states) for the substructures. Since the substructures are uncoupled ($\gamma = \alpha = 0$) and the controller is decentralized for this case, there is no cross coupling response. The figures also show a flat weighted closed-loop frequency response that is characteristic of optimal H_∞ controller response. In the transition bandwidths between the onset of performance rolloff (≈2 rad/s) and the onset of additive uncertainties (≈7 rad/s for substructures 1 and 2), rapid performance decay occurs.

2. Coupled SRCP, $\gamma = 1, \alpha = 0$: Cases 2 and 3

This configuration assumes a known fixed stiffness interface ($\gamma = 1, \alpha = 0$) between the two substructures. As in case 1, the higher frequency truncated component modes are the only model uncertainties assumed in this problem. The controller in case 2 is centralized whereas the controller in case 3 is decentralized. Only steps 1 and 2 of the sequential design was implemented for designing the decentralized robust controller in case 3. Controller order reduction at each step was done via balanced realization[35] for case 3.

Figure 15 shows the weighted closed-loop frequency responses from the combined disturbances to the outputs of interest when the structure is connected ($\gamma = 1, \alpha = 0$). A full model of the connected structure consisting of the first 30 modes was used in the open- and closed-loop frequency response. The open-loop response (dotted line) is shown for reference. At low frequencies, both controllers show excellent disturbance attenuation. Because of the controller constraint for case 3 (solid line), a performance degradation is significant, especially in the transition bandwidth and the cross transfer function.

The closed-loop response for the decentralized controller also shows strong coupling between disturbances from one substructure to the response of the other, although the controller itself is uncoupled. This implies significant structural coupling as evidenced by the magnitude of the off-diagonal open-loop response. This is surprising

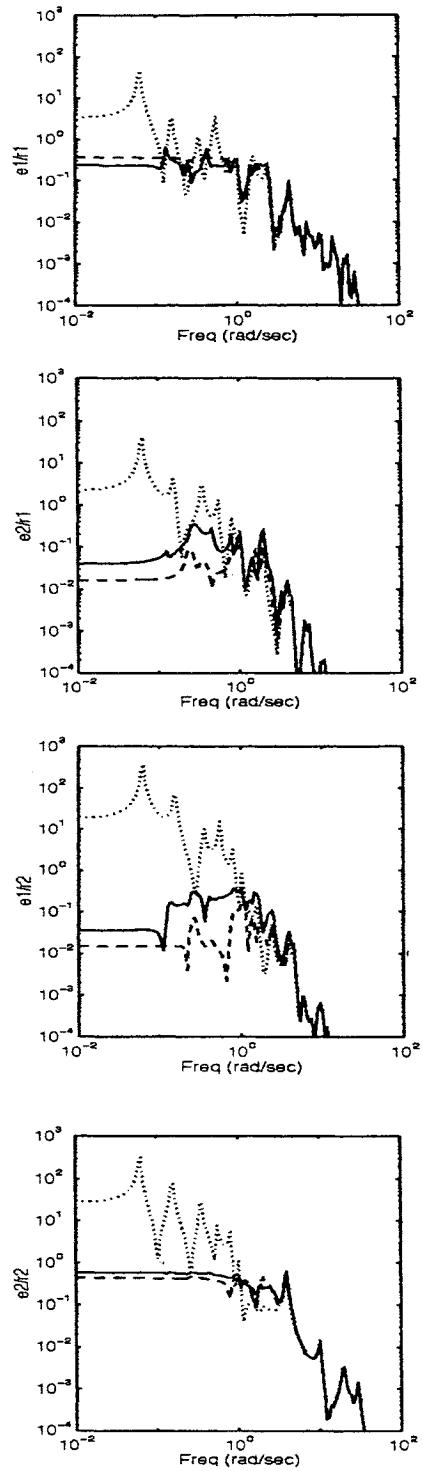

Fig. 15 Frequency response for cases 2 (dashed line) and 3 (solid line), $\gamma = 1$, $\alpha = 0$; open loop (dotted line).

since the nominal stiffness of the coupling section is two orders of magnitude less stiff than an equivalent length main substructure (see Table 1). In fact, cantilever beams have large excitability and detectability at the free ends due to the dominating fundamental structural mode response. When the two free ends are connected, even with a soft interface stiffness, the system is highly coupled as just described. Therefore, although the relative numerical values of interface coupling stiffness may indicate weak coupling, it is clear from the cross terms that it is not for this particular example.

3. Coupled SRCP, $\gamma = 1$, $|\alpha| \leq 1$: Cases 4 and 5

This configuration is the same as cases 2 and 3 except that the substructure interface stiffness is assumed to be uncertain and/or variable over a known range ($|\alpha| \leq 1$). The uncertainty in the interface

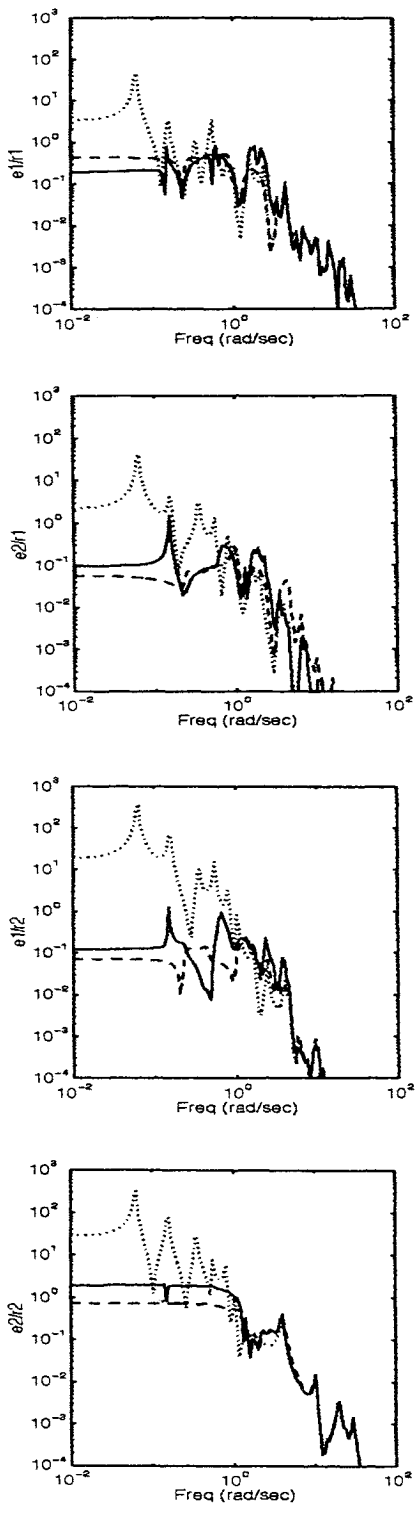

Fig. 16 Frequency response for cases 4 (dashed line) and 5 (solid line); open loop (dotted line); $\gamma = 1$, $\alpha = 0$.

stiffness is assumed to vary about a nominal of $\gamma = 1$, which gives the nominal interface stiffness

$$s_0 = \begin{bmatrix} -0.3 & -0.3 & 0.3 & -0.3 \\ -0.3 & -0.4 & 0.3 & -0.2 \\ 0.3 & 0.3 & -0.3 & 0.3 \\ -0.3 & -0.2 & 0.3 & -0.4 \end{bmatrix} \tag{28}$$

The nominal stiffness can be viewed as an intermediate stiffness condition between a fully coupled interface and where the two substructures are structurally uncoupled. From a physical standpoint, cases 4 and 5 are especially interesting because they cover the conditions

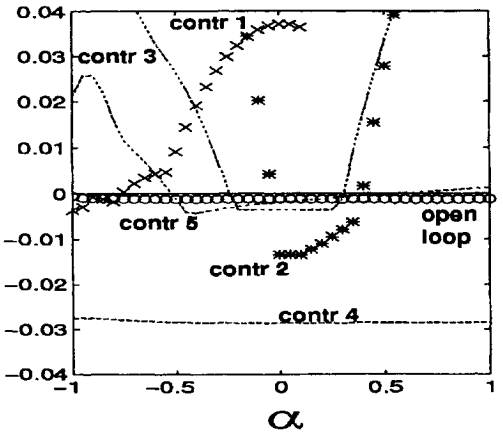

Fig. 17 Variation in largest real component of closed-loop eigenvalue with α at $\gamma = 1$; open loop (○), controllers 1 (×), 2 (∗), 3 (– – –), 4 (· · ·), 5 (– ·).

before ($\alpha = -1$), during ($-1 < |\alpha| < 1$), and after ($|\alpha| = 1$) docking using fixed (spatially decentralized for case 5) controllers. Steps 1–3 of the sequential design was implemented for designing the decentralized robust controller in case 5. Controller order reduction at each step was also done via balanced realization.

Figure 16 shows the weighted frequency response at nominal stiffness where $\alpha = 0$. The open-loop weighted frequency response (dotted line) is also shown for reference. Both controllers 4 and 5 gives good disturbance rejection at low frequencies but at transient and higher frequencies and for the cross transfer functions. The decentralized controller significantly loses performance due to its controller constraint. The figure also shows that the cross response (e_1/r_2 and e_2/r_1) is similar in magnitude to the local response (e_1/r_1 and e_2/r_2) even when the controller is decentralized for case 5.

4. Sensitivity to Interface Stiffness

The variations with α at $\gamma = 1$ in the largest real component of the closed-loop eigenvalues for all five controllers are shown in Fig. 17. A negative largest real component indicates stability, and the figure shows the approximate range of interface stiffness variation over which the closed-loop system remains stable using the evaluation model. Only controllers 4 and 5 are designed to accommodate specified variations in the interface stiffness. As expected, controller 1 (indicated by ×) remains stable in a small neighborhood about $\alpha = -1$ when the substructures are completely uncoupled. Controller 2 (indicated by ∗) remains stable in a small skewed neighborhood about $\alpha = 0$. Controller 3 (dashed line), which is the same as controller 2 except with decentralized control, gives a larger and more even neighborhood of stability than controller 2. Controller 4 (dotted line) is the only controller that guarantees robust stability over the whole range of α. With decentralization, controller 5 (dash–dot line) gives a smaller region of robustness than controller 4 but is still significantly larger than controllers 2 and 3.

Figure 18 shows the variation in the magnitude of the unweighted frequency response from input r_1 to output e_1 due to a change in interface stiffness for $\gamma = 1$, and $\alpha = (-0.4, 0, 0.4)$. The open-loop frequency response variation of the evaluation model is shown in Fig. 18a for reference. The changes in the interface stiffness significantly affect the frequency response of the structure over a wide frequency. Controller 1 was unstable for all three α values considered and is not shown. Controllers 2 and 3 were closed-loop unstable at $\alpha = -0.4$ and 0.4 and only the stable $\alpha = 0$ case is shown (dotted line). Controllers 4 and 5 were closed-loop stable for all three α values. This is not unexpected since they were the only controllers that accounted for the variation in the interface stiffness. Controller 4 gives the smallest variation (the three lines almost overlap) in the frequency response and is the most robust, as expected.

Figure 19 shows the dependence of the disturbance rejection performance (measured in terms of rms error) on interface stiffness. The left, center, and right bar plot for each controller show the rms value for $\alpha = -0.4, 0, 0.4$, respectively. Unstable responses are

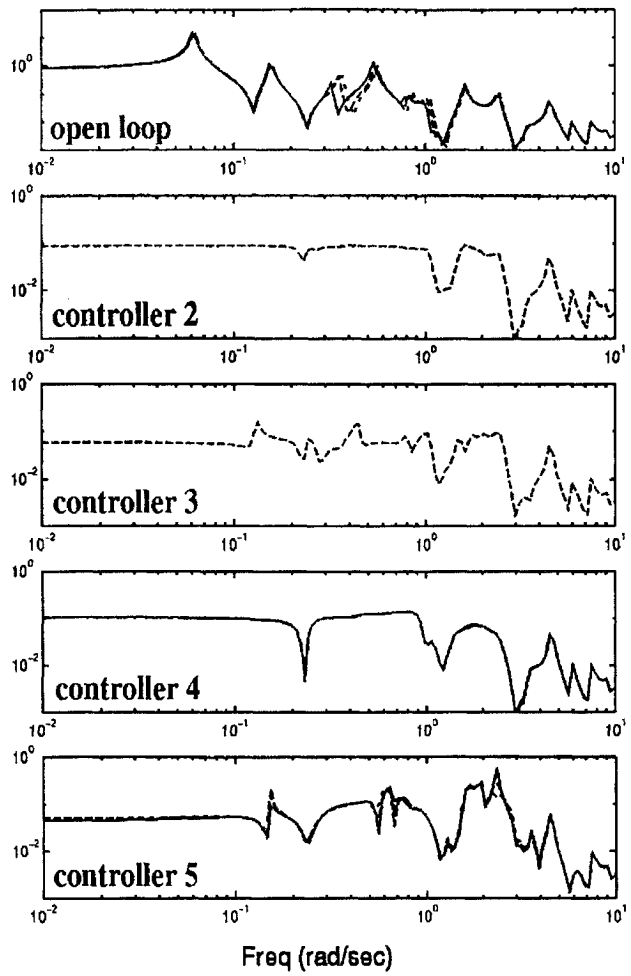

Fig. 18 Variation in frequency response (e_1/r_1) with interface stiffness, $\gamma = 1$, $\alpha = -0.4$ (solid line), 0 (dotted line), 0.4 (dashed line).

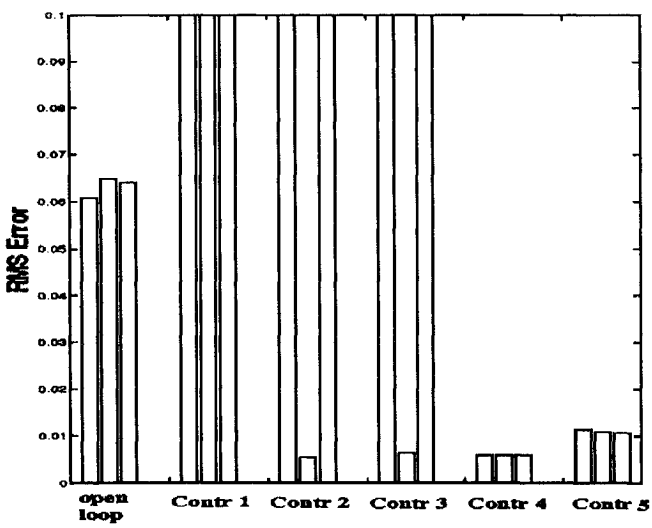

Fig. 19 Root-mean-square error dependence on interface stiffness $\alpha = -0.4$ (left), 0 (center), 0.4 (right).

denoted by 0.1 rms error in the figure. The rms errors for controllers 4 and 5 show only a small variation over the range of stiffness. There is a noticeable drop in rms performance for controller 5 due to controller decentralization. The nominal performance (at $\alpha = 0$) for controllers 2 and 3 are slightly better than controllers 4 and 5. This demonstrates the tradeoff in nominal performance for robustness over a larger set of structural configurations in the latter cases.

VII. Concluding Remarks

There is currently no established means to quantitatively account for model errors or uncertainties for a set of reduced component mode models. In response, a modularized control design framework has been proposed such that substructure data can be utilized directly. This development could prove useful because it takes advantage of the existing significant body of results in substructure modeling of large flexible structures. Although substructure controllers are highlighted, centralized controllers can also be directly designed from substructure data. In addition, synthesis of the substructures, as is usually done in component modes synthesis, is not necessary for control design.

Although the numerical examples are based on a one-dimensional structural system that is designed only to illustrate the proposed concept, they demonstrate a direct way to incorporate nominal substructure models and their corresponding uncertainties along with the substructure interface dynamics. The examples show that variations in the interface stiffness strongly affect stability and disturbance rejection performance. A small loss in nominal performance can be traded off for a significant gain in robustness. The results also demonstrate the feasibility of designing decentralized robust controllers by a sequential process, although decentralization significantly reduced performance. Of course, in the limiting case of uncoupled substructures, centralized controllers cannot perform any better than decentralized controllers.

Because of the 1-g testing environment, it may not be possible to test an assembled large flexible structure on the ground so that some comprehensive form of on-orbit system identification is critical. Since substructures can typically be tested independently in the laboratory, it is, in principle, possible to develop through testing component uncertainty models arising from inaccurate or reduced component modes and inconsistencies in the substructure boundary conditions. Perhaps the main advantage, then, in the proposed technique is in the reduction of the dependence on on-orbit system identification of the assembled structure by use of easier and less costly testing of substructures on the ground. In addition, control designs that are based on a single model of the assembled structure cannot be experimentally validated on ground. These controllers would also depend on nominal and uncertainty models that cannot be experimentally developed or validated.

The technique is particularly suited for large, complex, flexible structures that are weakly coupled. The degree of weakness in the coupling should exceed a threshold such that its overall stability cannot be guaranteed if decentralized controllers are designed independently or if its adjoining substructures are accounted for inaccurately. In addition, performance limitations due to controller decentralization should be significant. In practice, logistical constraints may make it impossible to implement a centralized controller.

Several important aspects of the coupled substructure robust control problem that are not adequately addressed and are open for further research include modeling substructural interfaces beyond static stiffness, optimal substructure model reduction, role of errors in the low-frequency modes of the subsystems, and quantification of the degree of suboptimality of the decentralized design.

Acknowledgments

The author would like to thank the anonymous reviewers for their many valuable comments in the revision of this paper.

References

[1]Cooper, P. A., et al., "Simulation of the Assembly Dynamics and Control of Space Station FREEDOM," AIAA Guidance, Navigation, and Control Conf., Monterey, CA, Aug. 1993.

[2]Garrison, J. L., Montgomery, R. C., Wu, S.-C., Ghosh, D., and Demeo, M. E., "Space Shuttle to Space Station FREEDOM Berthing Dynamics Research at the NASA Langley Research Center," 4th Conf. on Intelligent Robotic Systems for Space Exploration, Rensselaer Polytechnic Inst., Troy, NY, Sept.–Oct. 1992.

[3]Montgomery, R. C., et al., "A Testbed for Research on Manipulator-Coupled Active Spacecraft," AIAA Guidance, Navigation, and Control Conf., Monterey, CA, Aug. 1993.

[4]Davison, E. J., "The Robust Decentralized Control of a General Servomechanism Problem," *IEEE Transactions on Automatic Control*, Vol. AC-21, No. 1, 1976, pp. 14–24.

[5]West-Vukovich, G. S., and Davison, E. J., "The Decentralized Control of Large Flexible Space Structures," *IEEE Transactions on Automatic Control*, Vol. AC-29, No. 10, 1984, pp. 866–879.

[6]Davison, E. J., and Gesing, W., "Decentralized Control of Third Generation Spacecraft," American Control Conference, Minneapolis, MN, 1987, pp. 963–969.

[7]Joshi, S. M., *Control of Large Flexible Space Structures*, Vol. 131, Lecture Notes in Control and Information Sciences, Springer–Verlag, Berlin, 1989.

[8]Joshi, S. M., and Maghami, P. G., "Robust Dissipative Compensators for Flexible Spacecraft Control," *IEEE Transactions on Aerospace and Electronic Systems*, Vol. 28, No. 3, 1992, pp. 768–774.

[9]Vaz, A. F., and Davison, E. J., "The Structured Robust Decentralized Servomechanism Problem for Interconnected Systems," *Automatica*, Vol. 25, March 1989, pp. 267–272.

[10]Young, K. D., "Distributed Finite-Element Modeling and Control Approach for Large Flexible Structures," *Journal of Guidance, Control, and Dynamics*, Vol. 13, No. 4, 1990, pp. 703–713.

[11]Su, T.-J., and Craig, R. R., Jr., "Substructural Controller Synthesis," 3rd Annual Conf. on Aerospace Computational Control, Oxnard, CA, 1989.

[12]Su, T.-J., "A Decentralized Linear Quadratic Control Design Method for Flexible Structures," Ph.D. Dissertation, Dept. of Aerospace Engineering, Univ. of Texas, Austin, TX, 1989.

[13]Babuska, V., and Craig, R. R., Jr., "Substructure-Based Control of Flexible Structures," *AIAA 34th Structures, Structural Dynamics, and Materials Conference* (La Jolla, CA), AIAA, Washington, DC, 1993, pp. 3415–3422.

[14]Craig, R. R., Jr., and Bampton, M. C. C., "Coupling of Substructures for Dynamic Analysis," *AIAA Journal*, Vol. 7, No. 7, 1968, pp. 1313–1319.

[15]Craig, R. R., Jr., *Structural Dynamics—An Introduction to Computer Methods*, Wiley, New York, 1981.

[16]Meirovitch, L., *Computational Methods in Structural Dynamics*, Sijthoff and Noordhoof, Alphen aan den Rijn, The Netherlands, 1980.

[17]Spanos, J. T., and Tsuha, W. S., "Selection of Component Modes for Flexible Multibody Simulation," *Journal of Guidance, Control, and Dynamics*, Vol. 14, No. 2, 1991, pp. 278–286.

[18]Lim, K. B., Maghami, P. G., and Joshi, S. M., "A Comparison of Controller Designs for an Experimental Flexible Structure," *IEEE Control Systems*, Vol. 12, No. 3, 1992, pp. 108–118.

[19]Maciejowski, J. M., *Multivariable Feedback Design*, Addison–Wesley, Reading, MA, 1989.

[20]Doyle, J. C., "Analysis of Feedback Systems with Structured Uncertainties," *IEE Proceedings*, Pt. D, Vol. 129, 1982, pp. 242–250.

[21]Balas, G. J., and Doyle, J. C., "Robust Control of Flexible Modes in the Controller Crossover Region," American Control Conf., Pittsburgh, PA, June 1989.

[22]Balas, G. J., Doyle, J. D., Glover, K., Packard, A. K., and Smith, R., "μ-Analysis and Synthesis Toolbox," MUSYN Inc., Minneapolis, MN, April 1991.

[23]Doyle, J. C., "Structured Uncertainty in Control System Design," *Proceedings of the IEEE Conf. Decision Contr.*, 1985, pp. 260–265.

[24]Bathe, K.-J., *Finite Element Procedures in Engineering Analysis*, Prentice–Hall, Englewood Cliffs, NJ, 1982, Chap. 8.

[25]Sandell, N. R., Jr., Varaiya, P., Athans, M., and Safonov, M., "Survey of Decentralized Control Methods for Large Scale Systems," *IEEE Transactions on Automatic Control*, Vol. AC-23, No. 2, 1978, pp. 108–128.

[26]Mahmoud, M. S., Hassan, M. F., and Darwish, M. G., *Large-Scale Control Systems*, Marcel Dekker, New York, 1985.

[27]Larson, R. E., McEntire, P. E., and O'Riley, J. G., *Distributed Control*, IEEE Computer Society Press, Silver Spring, MD, 1982.

[28]Doyle, J. C., Lenz, K., and Packard, A., "Design Examples Using μ Synthesis: Space Shuttle Lateral Axis FCS During Reentry," *IEEE CDC*, Dec. 1986, pp. 2218–2223; also *Modelling, Robustness and Sensitivity Reduction in Control Systems*, edited by R. F. Curtain, NATO ASI Series, Vol. F34, Springer–Verlag, 1987, pp. 128–154.

[29]Packard, A., Doyle, J. C., and Balas, G. J., "Linear, Multivariable Robust Control with a μ Perspective," *Journal of Dynamics, Measurements and Control*, Special ed. on Control, Vol. 115, No. 2b, 1993, pp. 426–438.

[30]Stein, G., and Doyle, J. C., "Beyond Singular Values and Loopshapes," *Journal of Guidance, Control, and Dynamics*, Vol. 14, No. 1, 1991.

[31]Lim, K. B., and Balas, G. J., "Line-of-Sight Control of the CSI Evolutionary Model: μ Control," American Control Conf., Chicago, IL, June 1992.

[32]Lim, K. B., and Cox, D. E., "Experimental Robust Control Studies on an Unstable Magnetic Suspension System," American Control Conf., Baltimore, MD, June 29–July 1, 1994.

[33]Glover, K., and Doyle, J. C., "State-Space Formulae for all Stabilizing Controllers that Satisfy an H_∞ Norm Bound and Relations to Risk Sensitivity," *Systems and Control Letters*, Vol. 11, 1988, pp. 167–172.

[34]Doyle, J. C., Glover, K., Khargonekar, P., and Francis, B., "State-Space Solutions to Standard H_2 and H_∞ Control Problems," *IEEE Transactions on Automatic Control*, Vol. 34, No. 8, 1989.

[35]Moore, B. C., "Principal Component Analysis in Linear Systems: Controllability, Observability, and Model Reduction," *IEEE Transactions on Automatic Control*, Vol. AC-26, No. 1, 1981, pp. 17–32.